Progress of Theoretical Physics, Vol. 68, No. 6, December 1982

Analytic Solutions for Equilibrium of Rotating Isothermal Clouds

—— *One-Parameter Family of Axisymmetric and Conformal Configurations* ——

Chushiro HAYASHI, Shinji NARITA* and Shoken M. MIYAMA

Department of Physics, Kyoto University, Kyoto 606
**Department of Electronics, Doshisha University, Kyoto 602*

(Received June 29, 1982)

Equilibrium states of rotating axisymmetric isothermal gas clouds are studied and it is found that, if the linear rotation velocity is constant throughout a cloud, there exists a one-parameter family of conformal solutions which describe the equilibrium exactly. The parameter depends only on the ratio of the rotation velocity to the sound velocity and represents the flatness of equi-density contours in the direction of the rotation axis. Two extreme values of the parameter correspond to a non-rotating spherical configuration and a rapidly-rotating thin disk. Specific angular momentum on a cylindrical surface around the rotation axis is found to be proportional to the amount of mass contained inside the cylinder considered.

The stability of the equilibrium configurations is examined analytically as well as numerically and it is found that nearly spherical configurations are unstable to contraction and expansion as a whole, very flat configurations are unstable to ring formation and intermediate configurations are likely to be stable. Finally, these equilibrium configurations are compared with the results of numerical computations which have so far been performed by many people on the collapse of rotating isothermal clouds.

§ 1. Introduction

In connection with the problem of star formation, a great number of numerical computations have so far been performed on the gravitational collapse of rotating isothermal gas clouds (see, for example, a review article by Bodenheimer[1]). However, there still remain many questions as to the ultimate fate of the collapse, i.e., as to whether the collapse of the central part of a cloud continues unlimitedly or not and, furthermore, for what initial condition and at what stage a cloud fragments or reaches an equilibrium state. Here, the equilibrium means a balance of the three kinds of forces, gravity, gas pressure and centrifugal force.

In the present paper, we show that there exists a certain class of equilibrium states which is described by analytic solutions of a relatively simple form, as will be shown in § 2, and that these solutions throw some light on the questions mentioned above. In § 3, basic properties of these equilibrium configurations such as the distributions of gravity, mass and angular momentum will be described. In § 4, the stability of the configurations will be examined and, finally,

in § 5, discussion will be made of the ultimate fate of the collapse of rotating isothermal clouds.

In the remainder of this section, we describe a process of our discovery of the analytic solutions. Let us first consider the distribution of angular momentum in the initial state of a rotating isothermal cloud. Most of numerical computations of collapse, which have so far been made, start from a rigidly rotating sphere with uniform density, which satisfy Jeans' instability condition. For this initial state, let us consider a cylindrical surface with ϖ=constant (we adopt the cylindrical coordinates (ϖ, φ, z) where z denotes the rotation axis). The specific angular momentum $j(\varpi)$ on this surface is related to the mass $m(\varpi)$ contained inside the cylinder, according to

$$j=R^2\Omega_0\{1-(1-m/M)^{2/3}\}$$
$$=R^2\Omega_0(2m/3M)\{1+m/6M+(2/27)(m/M)^2+0(m^3/M^3)\}, \qquad (1\cdot1)$$

where R, M and Ω_0 are the total radius, the total mass and the rotational angular velocity of the initial cloud, respectively. It is seen from Eq. (1·1) that the ratio j/m is nearly constant if m/M is smaller than, say, 2/3.

Now, the ratio j/m is conserved in the course of collapse as long as the gas is inviscid and the axisymmetry is retained. The analytic solutions discovered by us correspond to a case where j/m is strictly constant throughout a cloud, as will be shown in § 3,

Recently, we have computed numerically the collapse of rotating clouds for the case of the sphere initial condition mentioned above as well as for the case of a disk initial condition proposed by Hayashi.[2] Our computations have been made with two different methods, i.e., a two-dimensional hydrodynamics code developed by Narita et al.[3] and a smoothed particle method which is similar to that used by Wood[4] but modified in some respects. The results of these computations will be published elsewhere. Now, the above disk initial condition is such that an isothermal disk, where gravity balances with gas pressure in the z-direction, is rotating with a constant angular velocity Ω_0 and a constant surface density ρ_{so}. In this case, instead of Eq. (1·1), we have

$$j=(\Omega_0/\pi\rho_{so})m\,, \qquad (1\cdot2)$$

and j/m is strictly constant.

In the course of our hydrodynamic computations performed for the disk initial condition with a small value of Ω_0, we found that gas density in the central part of a cloud increases unlimitedly with time and the cloud as a whole tends to have a density distribution which is nearly proportional to ϖ^{-2}. The same tendency was previously noticed by Norman et al.[5] in their computations for the case of the sphere initial condition. Furthermore, we found that equi-density

contours in the cloud become more and more flattened with time and the rotation velocity v_φ tends to be uniform throughout the cloud. These features together with the above j-m relation gave a clue for us to find the analytic solutions.

Now, we first consider a simple case of zero temperature, i.e., a case of an infinitely thin disk with an infinite extension in the ϖ-direction. We assume a surface density distribution of the power-law form

$$\rho_s(\varpi)=\hat{\rho}\,\varpi^{-n}, \quad (2>n>0) \tag{1·3}$$

where $\hat{\rho}$ and n are some constants. Then, it is found that the mass $m(\varpi)$ and the ϖ-component of gravity $F_\varpi(\varpi)$ are given by

$$m(\varpi)=2\pi\hat{\rho}\,\varpi^{2-n}/(2-n), \tag{1·4}$$

$$F_\varpi(\varpi)=-2\pi G\hat{\rho}k(n)\varpi^{-n} \tag{1·5}$$

with

$$k(n)=\Gamma(1-\frac{n}{2})\Gamma\left(\frac{1+n}{2}\right)\Big/\Gamma(\frac{n}{2})\Gamma\left(\frac{3-n}{2}\right), \tag{1·6}$$

where Γ denotes the gamma function. Then, from a condition that the disk under consideration is in equilibrium, i.e., the gravity is equal to the centrifugal force $j^2(\varpi)/\varpi^3$, we obtain a relation between $j(\varpi)$ and $m(\varpi)$, i.e.,

$$j=(2\pi G\hat{\rho}k(n))^{1/2}\{m(2-n)/2\pi\hat{\rho}\}^{(3-n)/2(2-n)}. \tag{1·7}$$

Furthermore, if we put a condition that the ratio j/m is constant throughout the disk, we find that $n=1$ and in this case the rotation velocity v_φ $(=j/\varpi)$ is constant. This is nothing but an equilibrium disk solution found by Mestel.[6] The generalization of this solution to the cases of finite temperatures, where the constancy of both j/m and v_φ is preserved, will be described in the next section.

§ 2. Derivation of equilibrium solutions

We use mainly the cylindrical coordinates (ϖ, φ, z) but also sometimes use the corresponding spherical coordinates (r, θ, φ) and the rectangular coordinates (x, y, z). We consider an equilibrium state of an isothermal cloud which is axially as well as equatorially symmetric and rotating with a constant velocity v_φ. The balance of gravity, gas pressure and centrifugal force in the ϖ- and z-direction is written as

$$F_\varpi=c^2\partial\ln\rho/\partial\varpi-v_\varphi{}^2/\varpi, \tag{2·1}$$

$$F_z=c^2\partial\ln\rho/\partial z, \tag{2·2}$$

where $c=(P/\rho)^{1/2}$ is the sound velocity and ρ is the gas density. Furthermore,

we have the Poisson equation for F_ϖ, F_z and ρ. Putting

$$\rho(\varpi, z)=g(\varpi, z)/\varpi^2 \tag{2·3}$$

and using Eqs. (2·1) and (2·2), we can write the Poisson equation in the form

$$\varpi\frac{\partial}{\partial\varpi}\left(\varpi\frac{\partial \ln g}{\partial\varpi}\right)+\varpi\frac{\partial}{\partial z}\left(\varpi\frac{\partial \ln g}{\partial z}\right)=-4\pi Gg/c^2 . \tag{2·4}$$

Since Eq. (2·4) is invariant to the scale changes of both ϖ and z, it has a conformal solution such that g is a function of z/ϖ alone. Then, putting

$$z/\varpi=\sinh\zeta=\cot\theta \tag{2·5}$$

or

$$\zeta=\ln\{(r+z)/\varpi\}=\ln\{(1+\cos\theta)/\sin\theta\}, \tag{2·6}$$

we obtain a simple equation for $g(\zeta)$, i.e.,

$$d^2 \ln g/d\zeta^2=-(4\pi G/c^2)g . \tag{2·7}$$

All the solutions of this equation which satisfy the boundary condition that g is finite and $dg/d\zeta=0$ at $\zeta=0$ are given by

$$g(\zeta)=\gamma^2c^2/\{2\pi G\cosh^2(\gamma\zeta)\}, \tag{2·8}$$

where γ is an arbitrary constant which will be determined in the following.

From Eqs. (2·1), (2·2), (2·3) and (2·8), the gravity in the immediate neighborhood of the z-axis is given by

$$(\varpi F_\varpi)_{\varpi\to 0}=-2c^2(1+v_\varphi^2/2c^2-\gamma), \tag{2·9}$$

$$(F_z)_{\varpi\to 0}=-2\gamma c^2/z . \tag{2·10}$$

Now, applying Gauss' divergence theorem to a narrow tube enclosing the z-axis, we find that, in general cases, a mass string exists on the z-axis with the line density

$$\rho_l=(c^2/G)(1+v_\varphi^2/2c^2-\gamma). \tag{2·11}$$

This line density is uniform and gives, in general, an infinite mass if integrated all over the z-axis. Then, from a condition that this mass should vanish, we obtain a relation between γ and the Mach number v_φ/c, i.e.,

$$\gamma=1+v_\varphi^2/2c^2 . \tag{2·12}$$

Equi-density surfaces in the x-z plane, which are given by Eqs. (2·3) and (2·8), are shown in Figs. 1 and 2 for several values of γ. The constant γ denotes the flatness of the equi-density surfaces, as shown in Fig. 2, and will be called the

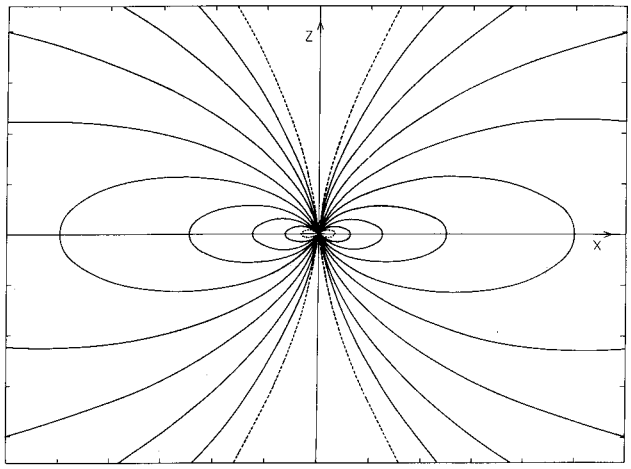

Fig. 1. Equi-density contours in the x-z plane in the equilibrium configuration with $\gamma=3$.

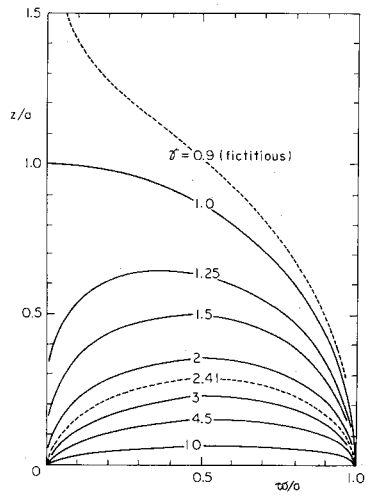

Fig. 2. Shapes of equi-density contours in the ϖ-z plane for different values of γ. The dotted curve with $\gamma=0.9$ denotes a fictitious case where a negative mass exists on the z-axis.

flatness parameter hereafter. We have two limiting cases, $\gamma=1$ and $\gamma=\infty$. The former is a non-rotating spherical configuration with the density distribution, $\rho=c^2/2\pi Gr^2$, which is very similar to that found by Larson[7] and many others in numerical computations of the collapsing spherical isothermal clouds. The latter is the Mestel solution mentioned at the end of § 1. Properties of the equilibrium solutions, other than the density distribution, will be described in the next section.

§ 3. Properties of equilibrium solutions

The equilibrium solutions found in § 2 have a very simple expression for the density, i.e.,

$$\rho=\gamma^2c^2/(2\pi G\varpi^2\cosh^2\gamma\zeta), \tag{3·1}$$

but this is not always the case for the other quantities such as the distributions of gravity, mass and angular momentum. Then, it will be worth while to summarize the results of our calculations in this section.

(1) *Distributions of gravity, surface density and mass*

With Eq. (2·12) we find for the components of gravity

$$\left.\begin{aligned} F_\varpi &= -(2\gamma c^2/\varpi)(1-\tanh\zeta\tanh\gamma\zeta), \\ F_z &= -(2\gamma c^2/\varpi)\tanh\gamma\zeta/\cosh\zeta, \end{aligned}\right\} \tag{3·2}$$

$$\left.\begin{aligned} F_r &= -2\gamma c^2/r, \\ F_\theta &= (2\gamma c^2/r)\sinh(\gamma-1)\zeta/\cosh\gamma\zeta. \end{aligned}\right\} \tag{3·3}$$

From these equations, the gravity potential ϕ is found to be given by

$$\phi = 2c^2\ln(\varpi^\gamma\cosh\gamma\zeta) = 2c^2\ln\left\{\frac{1}{2}(r+z)^\gamma+\frac{1}{2}(r-z)^\gamma\right\}, \tag{3·4}$$

except for an additional constant. We can confirm Eq. (3·4) by direct integration of the Poisson equation using Eq. (3·1) and the Green function as given by Eq. (4·9) but the proof is omitted here. The lines of gravity force which are perpendicular to the equi-potential surfaces are given by

$$\varpi^{\gamma-1}/\sinh(\gamma-1)\zeta = \text{constant}. \tag{3·5}$$

For example, in a special case $\gamma=2$, the equi-potential surfaces and the gravity lines are expressed simply as, $\varpi^2+2z^2=$const and $\varpi^2/z=$const, respectively. In the case $\gamma=\infty$, the equi-potential surfaces are expressed in the simple form, $r+z=$const, which indicates that the equi-potential surfaces are not flat although the disk itself is infinitely thin.

Now, carrying out the integration of density over z (where it is convenient to use the variable, $\eta=\exp(2\gamma\zeta)$, instead of ζ), we find that the surface density is given by

$$\rho_s(\varpi) = \int_{-\infty}^{\infty}\rho(\varpi, z)dz = (\gamma c^2/\pi G\varpi)f_1(\gamma) \tag{3·6}$$

with

$$f_1(\gamma) = \Gamma(1+1/2\gamma)\Gamma(1-1/2\gamma) = (\pi/2\gamma)/\sin(\pi/2\gamma). \tag{3·7}$$

Next, we consider four different axisymmetric surfaces, (1) the cylindrical surface, (2) the spherical surface, (3) the equi-potential surface and (4) the equi-density surface as shown in Fig. 3, all of which contact each other on the same equator with the radius ϖ. Let the amounts of mass contained in regions inside the four surfaces be denoted by $m_i(\varpi)$ with $i=1, 2, 3$ and 4, respectively. Then, we find that these masses are all expressed in the same form

$$m_i(\varpi) = 2\gamma c^2\varpi f_i(\gamma)/G, \qquad (i=1, 2, 3, 4) \tag{3·8}$$

where f_1 is given by Eq. (3·7) and the other f_i's are given by

$$f_2=1, \quad f_3=2^{1/\gamma}/(1+1/\gamma)$$

and

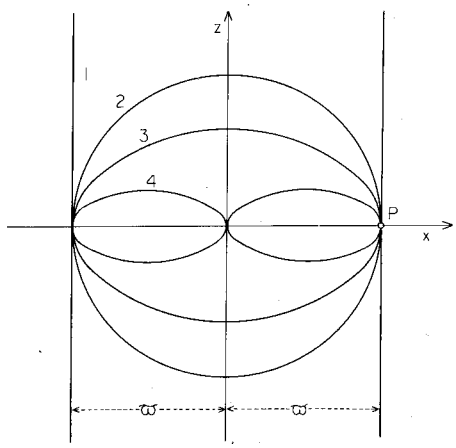

Fig. 3. Cross sections of four different axisymmetric surfaces for the case $\gamma=3$.

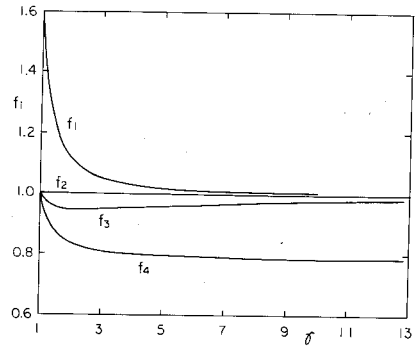

Fig. 4. The values of f_1, f_2, f_3 and f_4 as functions of γ.

$$f_4=\Gamma(3/2+1/2\gamma)\Gamma(3/2-1/2\gamma)=(\pi/4)(1-1/\gamma^2)/\cos(\pi/2\gamma). \qquad (3\cdot9)$$

It is to be noticed that the above masses $m_i(\varpi)$ are all proportional to ϖ and vanish as $\varpi\to0$ although the density is infinite at the origin. The values of f_i as functions of γ are plotted in Fig. 4, which indicates that $f_1-f_4\simeq0.2f_4$, i.e., the mass contained outside the equi-density surface is small as compared with that contained inside this surface. Now, in the case of isothermal clouds a way to obtain equilibrium configurations of finite size is to introduce a small but finite external pressure. Then, in order to see the degree of variation of the configuration caused by the introduction of a constant external pressure, we have computed numerically how much the gravity changes in regions inside the equi-density surface when the mass outside this surface is all removed. We have found that in the case $\gamma=6$ the increase of gravity is, at most, 10 percent and, thus, we can expect that the equilibrium configurations found by us are not much affected by the introduction of a constant external pressure.

If this is the case, we can obtain from Eqs. (3·1) and (3·8) a relation between the external pressure P_E and the total mass $M(=m_4)$ of an isothermal cloud which is in equilibrium. The result is given by

$$M=(2c^6/\pi G^3\rho_E)^{1/2}\gamma^2 f_4(\gamma), \qquad (3\cdot10)$$

where $\rho_E=P_E/c^2$ is the density at the outer boundary of the cloud and $f_4(\gamma)$ is given by Eq. (3·9). This mass is to be compared with the critical maximum mass of the Emden solution of a spherical cloud (see, for example, a book of Spitzer[8]), i.e.,

$$M=1.18(c^6/G^3\rho_E)^{1/2}. \qquad (3\cdot11)$$

It is likely that our equilibrium configurations with γ lying between 2.4 and about 7 are stable, as will be shown in § 4. Then, we find for the case $\gamma=7$ that Eq. (3·10) gives a mass about 26 times greater than Eq. (3·11). Namely, when the cloud is rotating, such a large mass can be supported by centrifugal force. Thus, the stability of our equilibrium configurations is very important not only for the problem of star formation but also for the study of the structure and lifetime of molecular clouds in our galaxy.

(2) *Column densities and optical depths*

We consider the optical depth of the point P as shown in Fig. 3. Column densities along straight lines which start from the same point P and extend to plus infinites in the x-, y- and z-direction are given by

$$\sigma_x=\gamma^2c^2/2\pi G\tilde{\omega},\quad \sigma_y=\pi\sigma_x/2 \quad\text{and}\quad \sigma_z=(\pi/2\gamma^2)\sigma_x/\sin(\pi/2\gamma), \tag{3·12}$$

respectively, where σ_z is, of course, equal to a half of $\rho_s(\tilde{\omega})$ as given by Eq. (3·6). It will be found from Eq. (3·12) that, for any value of γ, the optical depth of the point P is practically given by $\varkappa\sigma_z$ where $\varkappa$ is the opacity which is assumed to be constant. Then, the condition that the point P is optically thin, i.e., $\varkappa\sigma_z\leq 1$, is written in the form

$$\rho(\tilde{\omega}, z=0)\leq 1.2\times10^{-14}\varkappa^{-2}T^{-1}\ \mathrm{g\ cm^3}, \tag{3·13}$$

$$m_1(\tilde{\omega})/M_\odot\geq 4.4\times10^{-5}\varkappa\gamma^2T^2, \tag{3·14}$$

where we have used Eqs. (3·1) and (3·8), put $c^2=kT/\mu m_H$ with $\mu=2.35$ and expressed all the quantities in c.g.s. units.

For example, if we consider a case $m_1=1M_\odot$, we have from Eq. (3·14)

$$\gamma\leq 150\varkappa^{-1/2}T^{-1}, \tag{3·15}$$

and the opacity $\varkappa$, which is due mainly to dust grains, is about 0.01 and 0.1 $\mathrm{cm^2g^{-1}}$ for $T=10$ and 20 K, respectively. Then, γ is to be smaller than about 150 and 24 (see the dashed line in Fig. 5), respectively, in order that a cloud of $1M_\odot$ be optically thin and, thus, the isothermal assumption be valid.

(3) *Angular momentum distribution and its relation to the initial condition*

The ratio of the specific angular momentum $j(\tilde{\omega})$ $(=\tilde{\omega}v_\varphi)$ to the mass $m_1(\tilde{\omega})$ is given by

$$j(\tilde{\omega})/m_1(\tilde{\omega})=(G/\pi c)\{2(\gamma-1)\}^{1/2}\sin(\pi/2\gamma). \tag{3·16}$$

This ratio depends only on the flatness parameter γ and is constant throughout an equilibrium configuration.

Now, we consider a relation of this angular momentum distribution to that of

the initial state of a collapsing cloud as described in § 1. In general, the collapsing cloud has finite velocity components in the ϖ- and z-direction and in the course of collapse these velocities will decay, soon or later, owing to shock wave generation. Then, we assume that the cloud finally reach an equilibrium state with the conservation of angular momentum. This conservation will be complete if the gas is inviscid and also the axisymmetry is preserved during the collapse.

First, we consider the disk initial condition, as described in § 1, where both the surface density ρ_{so} and the rotational angular velocity Ω_0 are constant. In this case, the initial value of j/m is given by Eq. (1·2) and comparing this with Eq. (3·16) we find that the angular momentum is strictly conserved if

$$c\Omega_0/G\rho_{so}=\{2(\gamma-1)\}^{1/2}\sin(\pi/2\gamma). \tag{3·17}$$

This relation is plotted in Fig. 5, which indicates that the curve takes a peak value 1.019 at $\gamma=2.411$ and two equilibrium configurations exist for the same value of Ω_0/ρ_{so}. Especially, in the case of very small Ω_0, we have a spherical configuration ($\gamma\simeq1$) as well as a very flat configuration ($\gamma\gg1$).

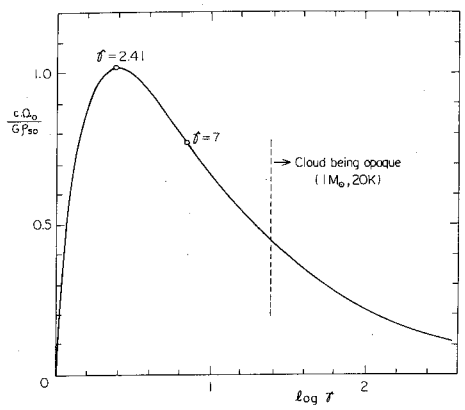

Fig. 5. Relation between the disk initial condition and the corresponding equilibrium solution. Here, Ω_0 and ρ_{so} denote the angular velocity and the surface density of the initial disk.

As will be shown in § 4, equilibrium configurations with $\gamma<2.41$ are unstable to a nearly homologous contraction while very flat configurations with $\gamma\gtrsim7$ are unstable to ring formation and, probably, also to fragmentation. Then, there arises a question as to whether the fragmentation occurs after or before the cloud reaches an equilibrium state. This question is to be answered by numerical computations in the near future.

Second, we consider a relation to the sphere initial condition where both the density and the rotational angular velocity Ω_0 are constant. In this case, the initial condition is specified by the two parameters,

$$\alpha=E_t/|E_g|=5c^2R/2GM \quad \text{and} \quad \beta=E_r/|E_g|=\Omega_0^2R^3/3GM\,, \tag{3·18}$$

where E_t, E_g and E_r are the thermal, gravitational and rotational energies of a whole cloud, respectively. The initial value of j/m is given by Eq. (1·1). Comparing the dominant term in this equation, i.e., the term proportional to m,

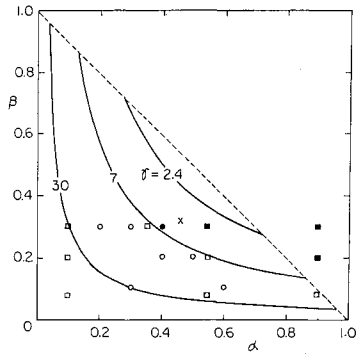

Fig. 6. Relation between the initial condition parameters, α and β, and the flatness parameter γ of equilibrium solutions. The dashed line denotes the condition of zero binding energy. The initial conditions of Boss and Haber are denoted by the open squares (ring cases) and the closed squares (no ring cases). Those of Wood are denoted by the open circles (fragmentation cases) and the closed circle (fragmentation is not obvious). The cross denotes our calculation (no ring).

with Eq. (3·16) and using Eq. (3·18), we have for the conservation of angular momentum

$$\pi(8\alpha\beta/15)^{1/2}=\{2(\gamma-1)\}^{1/2}\sin(\pi/2\gamma). \tag{3·19}$$

This relation is shown in Fig. 6, where the curves of constant γ (≥ 2.41) are drawn in the α-β plane.

Now, the results of numerical computations, which have so far been made with the sphere initial condition, will be compared with the instability criteria for the equilibrium solutions as mentioned above. For example, the results of Boss and Haber[9] with two-dimensional hydrodynamic code show that a cloud collapses and forms a ring in several cases (denoted by the open squares in Fig. 6). However in their other cases (the closed squares in Fig. 6), a cloud reaches a disklike equilibrium and there is no ring formation. Recent computations by Wood[10] with a smoothed particle method indicate that, in six cases (denoted by the open circles in Fig. 6) where we have $\gamma>7$, a cloud finally fragments into two or three pieces while, in one case (the closed circle in Fig. 6) corresponding to $\gamma=6.5$, the fragmentation is not obvious. Furthermore, we have confirmed with our own computation that ring formation does not occur for a case $\alpha=0.46$ and $\beta=0.32$, i.e., $\gamma=4.9$ (the cross in Fig. 6). Thus, the above examples indicate that the collapse of a cloud with the sphere initial condition leads to fragmentation or ring formation if $\alpha\beta\lesssim 0.11$, i.e., if $\gamma\gtrsim 7$ according to Eq. (3·19). This means that the fragmentation or the ring formation occurs at a stage where the cloud nearly reaches an equilibrium state. Anyhow, further numerical computations are necessary before we obtain a definite conclusion.

§ 4. Stability of the equilibrium configurations

The equilibrium configurations, described in §§ 2 and 3, are two-dimensional and have an infinite extension as well as a point singularity at the center. It is

difficult to obtain a complete stability criterion for such configurations and, then, we have studied the stability for the following three cases. The first is a simple case of a spherical configuration with $\gamma=1$. The second is a test of instability with an energy principle for nearly spherical cases with $\gamma\lesssim 2$ where the expansion of gravity potential in Legendre polynomials is effective. The third is a test for the growth of a ring-mode perturbation for cases of large $\gamma(>4)$ by means of numerical computations with our hydrodynamic code.

(1) *A spherical configuration*

We assume that a constant external pressure, P_E, is acting on the outer boundary, $r=R$, and consider the growth of a spherically-symmetric perturbation, which is not necessarily small. From the equations of continuity and motion for an isothermal cloud, we have the integral

$$K=\int_0^M v_r^2/2\,dm=\int_0^M(Gm/r-c^2\ln\rho)dm-4\pi R^3P_E/3+\text{const}\,, \qquad (4\cdot1)$$

where m is the mass contained inside a sphere with radius r and v_r is the radial velocity. We adopt, in the following, the Lagrangian scheme and consider m as an independent variable.

The density at the outer boundary, $\rho_E=P_E/c^2$, is to be kept constant and we consider the distribution of density in the inner regions, which is expressed in the power-law form

$$\rho/\rho_E=(m/M)^{-2-3l}\,, \qquad (4\cdot2)$$

where l is a constant which measures the degree of density variation from the equilibrium configuration where $l=0$. The radius r corresponding to the above density distribution is given by

$$r=\{M/4\pi\rho_E(1+l)\}^{1/3}(m/M)^{1+l}\,, \qquad (4\cdot3)$$

and we can calculate the kinetic energy K, given by Eq. (4·2), as a function of l. The result is

$$\begin{aligned}(1/c^2M)(K(l)-K(0))&=2\left\{\frac{(1+l)^{1/3}}{1-l}-1\right\}-3l-\frac{1}{3}\left(\frac{1}{1+l}-1\right),\\&=19l^2/9+235l^3/81+O(l^4)\end{aligned}$$

$$\text{for}\quad |l|\ll 1\,. \qquad (4\cdot4)$$

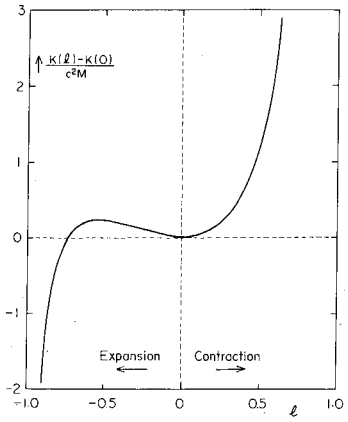

Fig. 7. The variation of the kinetic energy $K(l)$ as a function of the deformation parameter l.

As shown in Fig. 7, the kinetic energy increases with the progress of contraction ($l>0$) and also expansion ($l<0$), but in the case of expansion a cloud has to turn to contraction at $l=-0.75$. Thus, the equilibrium configuration is found to be unstable for the contraction and expansion of a cloud as a whole.

(2) *Nearly spherical configurations with $\gamma \lesssim 2$*

We use the spherical coordinates with $x=(r, \mu)$, where $\mu=\cos\theta$, and consider small axisymmetric displacements of material elements from their equilibrium positions. The displacement is denoted by $\boldsymbol{\xi}=(\xi_r, \xi_\mu)$ and the perturbed velocity is given by $\boldsymbol{u}=\partial\boldsymbol{\xi}/\partial t$. Then, linearized equations of continuity and motion in the Eulerian scheme are written as

$$\frac{\partial^2\xi_r}{\partial t^2}=-2\frac{{v_0}^2}{r^2}\left(\xi_r-\frac{\mu r}{1-\mu^2}\xi_\mu\right)-\frac{\partial}{\partial r}\left(c^2\frac{\rho_1}{\rho_0}+\phi_1\right), \tag{4·5}$$

$$\frac{\partial^2\xi_\mu}{\partial t^2}=2\frac{{v_0}^2}{r^3}\mu\left(\xi_r-\frac{\mu r}{1-\mu^2}\xi_\mu\right)-\frac{1-\mu^2}{r^2}\frac{\partial}{\partial\mu}\left(c^2\frac{\rho_1}{\rho_0}+\phi_1\right) \tag{4·6}$$

with

$$\rho_1=-\mathrm{div}(\rho_0\boldsymbol{\xi})=-(1/r^2)\partial(\rho_0 r^2\xi_r)/\partial r-\partial(\rho_0\xi_\mu)/\partial\mu\,, \tag{4·7}$$

$$\phi_1(\boldsymbol{x})=\int H(\boldsymbol{x}, \boldsymbol{x}')\rho_1(\boldsymbol{x}')d\tau'\,, \quad d\tau=2\pi r^2 dr d\mu\,, \tag{4·8}$$

$$H(\boldsymbol{x}, \boldsymbol{x}')=-G\sum_{n=0}^{\infty}P_n(\mu)P_n(\mu')H_n(r, r'), \tag{4·9}$$

$$H_n(r, r')=1/r(r'/r)^n \quad (\text{for } r>r'), \qquad 1/r'(r/r')^n \quad (\text{for } r<r'), \tag{4·10}$$

where v_0 and ρ_0 are unperturbed rotational velocity and density, respectively, ϕ_1 is the perturbed potential and $P_n(\mu)$ denotes Legendre polynomials.

If we put $\xi\propto e^{i\omega t}$, the above equations take a form of the eigenvalue equation, i.e.,

$$\rho_0\omega^2\xi_i=\sum_k \Lambda_{ik}\xi_k\,, \qquad (i, k=1, 2) \tag{4·11}$$

where Λ_{ik} is a self-adjoint integro-differential operator and it is well-known that the eigenvalue ω^2 is real. Furthermore, the minimum eigenvalue is given by

$$\omega^2=\min(A/B) \tag{4·12}$$

with

$$A=\sum_{i,k}\int\xi_i\Lambda_{ik}\xi_k d\tau \quad \text{and} \quad B=\sum_i\int{\xi_i}^2\rho_0 d\tau\,. \tag{4·13}$$

This is the well-known energy principle utilized for the estimation of ω^2 of the most dangerous mode of perturbations. Namely, if we expand the sum of rotational, thermal and gravitational energies of a system under consideration into a power series of ξ as

$$E=E_0+E_1(\xi)+E_2(\xi^2)+\cdots, \tag{4·14}$$

the condition, $\delta E=0$, gives the equations for equilibrium and E_2 is equal to a half of A, which is given by Eq. (4·13).

In the present case, from Eqs. (4·5) to (4·10) we have

$$A=2v_0^2\int\left(\xi_r-\frac{\mu r}{1-\mu^2}\xi_\mu\right)^2\frac{\rho_0 d\tau}{r^2}+c^2\int(\mathrm{div}\,\rho_0\boldsymbol{\xi})^2\frac{d\tau}{\rho_0}$$
$$+\int\mathrm{div}(\rho_0\boldsymbol{\xi})H(\boldsymbol{x},\boldsymbol{x}')(\mathrm{div}\,\rho_0\boldsymbol{\xi})'d\tau d\tau', \tag{4·15}$$

$$B=\int\left(\xi_r^2+\frac{r^2}{1-\mu^2}\xi_\mu^2\right)\rho_0 d\tau, \tag{4·16}$$

where the dash denotes taking a value at $\boldsymbol{x}'$. Now, we consider a special mode such that

$$\xi_r=\xi(r) \quad \text{and} \quad \xi_\mu=0. \tag{4·17}$$

Then, we have

$$(G/2\gamma c^2)A=\int\{2v_0^2(\xi^2/r^2)+c^2(d\xi/dr)^2\}dr$$
$$-2\gamma c^2\sum_{n=0}^{\infty}\int g_n^2(\gamma)H_n(r,r')(d\xi/dr)(d\xi/dr)'drdr' \tag{4·18}$$

with

$$g_n(\gamma)=\gamma/2\int_{-\infty}^{\infty}P_n(\mu)/\cosh^2(\gamma\zeta)d\zeta, \tag{4·19}$$

where γ is the flatness parameter and we have a relation, $\mu=\tanh\zeta$, according to Eq. (2·5).

The integral in Eq. (4·19) takes simple values in special cases, i.e.,

$$g_0(\gamma)=1 \quad \text{and} \quad g_n(1)=\begin{cases}1, & (n=0)\\ 0. & (\text{otherwise})\end{cases} \tag{4·20}$$

In a case $\gamma=2$, we have for the series in Eq. (4·18)

$$\sum_{n=0}^{\infty}g_n^2(\gamma=2)H_n=H_0+0.0827H_2+0.0040H_4+\cdots, \tag{4·21}$$

and it is seen that, for $\gamma \lesssim 2$, the first term H_0 has a major contribution. Furthermore, from Eq. (4·10) we find for H_0

$$\partial^2 H_0(r, r')/\partial r \partial r' = \delta(r-r')/r^2 , \tag{4·22}$$

where δ denotes Dirac's delta function.

Now, considering the cases with $\gamma \lesssim 2$ and retaining only the term H_0, we have

$$(G/2\gamma c^2)A = \int \{2(\gamma-2)\xi^2 r^{-2} + (d\xi/dr)^2\} dr . \tag{4·23}$$

This indicates that, for $\gamma < 2$, A can be negative for large-wavelength perturbations such that $|d\xi/dr|^2 \ll |\xi/r|$. Namely, equilibrium configurations with $\gamma < 2$ are unstable for the growth of such nearly-spherical long-wave perturbations but stable against small-wavelength perturbations such as to form spherical shells. Furthermore, it is expected that, if the higher terms H_2, H_4, etc. are included, the critical value of γ for instability will increase from 2 to a slightly larger value, say, 2.4. The exact value is expected to be 2.411, in view of the fact that there exist two different equilibrium configurations for the same value of j/m, as shown in Fig. 5. On the other hand, in the cases of flattened configurations with γ larger than, say, 4, the convergence of the series, $\sum_n g_n^2 H_n$, is not good. Then, we have tested the stability by means of direct numerical computations, as will be described in the following.

(3) *Test of ring-mode stability with numerical computations*

In this section, ring-mode stability of a family of the equilibrium solutions is investigated using our two-dimensional hydrodynamics code. The computational method of the code has been revised in some respects but nearly similar to that described by Narita et al.,[3] which is based on the Fluid-in-Cell method with the spherical-polar coordinates. The adopted mesh number for this test is 100 (in the r-direction) times 13 (in the θ-direction) and the mesh parameter, r_{i+1}/r_i, is 1.05.

The initial mode of perturbation is given by a function of r alone for simplicity. This restriction of the mode does not seem to be too serious because it is found below that ring-mode instability occurs only in rather thin disk configurations.

For the first test, the displacement of material from the unperturbed position, r_0, to r is given by

$$r - r_0 = -\frac{\varepsilon}{k} \sin kr , \tag{4·24}$$

where ε is a small numerical coefficient. Since the unperturbed values of the

density, ρ_0, and the angular velocity, ω_0, are proportional to r_0^{-2} and r_0^{-1}, respectively, their perturbed values are represented by

$$\rho(r, \theta)=\rho_0(r, \theta)(1+\varepsilon \cos kr) \tag{4·25}$$

and

$$\omega(r, \theta)=\omega_0(r, \theta)\left(1+\frac{\varepsilon}{kr} \sin kr\right), \tag{4·26}$$

using the conservation laws of mass and angular momentum.

Now, we compare the differences of the magnitudes of the forces between the unperturbed and the perturbed state in the equatorial plane of the cloud. If the difference of the gravity overcomes the sum of those of the centrifugal force and the gas pressure, the perturbation is expected to be enhanced and vice versa. The unperturbed density distribution given by Eq. (3·1) is rewritten in the spherical-polar coordinates as

$$\rho_0(r, \theta)=\frac{2c^2\gamma^2}{\pi G r^2} \frac{(1-\cos^2\theta)^{\gamma-1}}{\{(1+\cos\theta)^\gamma+(1-\cos\theta)^\gamma\}^2}. \tag{4·27}$$

This configuration is, unfortunately, not exactly in equilibrium because it has an outer boundary in the code. The boundary condition, however, may not cause any remarkable effect as far as the differences between the two states are concerned and also as far as the perturbation is small and lies in the deep interior of the cloud. The computation has been carried out when $\varepsilon=0.05$ and $\gamma=40$, 20, 10 and 6.

The computational results show that ring-mode instability seems to take place in the region where

$$\lambda/\varpi \gtrsim 7/\gamma, \tag{4·28}$$

where ϖ denotes the distance from the rotation axis and λ the wavelength of the perturbation, $2\pi/k$. Actually, the numerical factor in Eq. (4·28) changes slightly with respect to γ. It is about 6.5 for $\gamma=40$ and 20, and 8 for $\gamma=10$. When $\gamma=6$, it has been found that this ring-mode perturbation will be diminished with any wavelength. We may expect from these results that a cloud is stable against ring-mode perturbations when $\gamma \lesssim 7$ because λ cannot be much larger than ϖ.

In reality, however, the displacement of material in the r-direction necessarily induces the motion in the θ-direction which may enhance the perturbation. The perturbed motion may also propagate in the inward as well as the outward direction and develop. Therefore, the second test has been performed in which time development of the perturbation was investigated. In this test, velocity perturbation instead of the displacement of material is given initially in the r-direction in the unperturbed configuration by

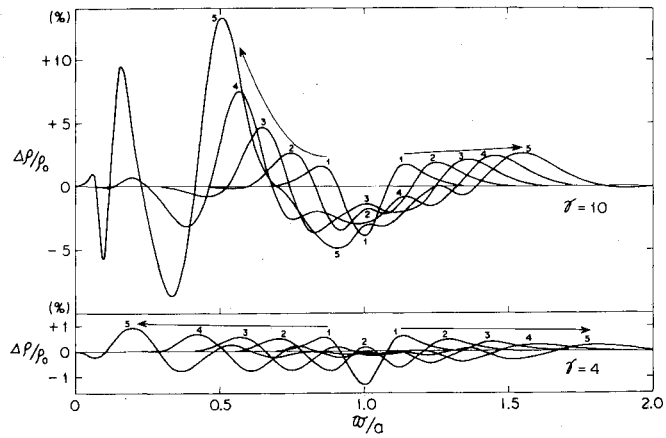

Fig. 8. The time variation of the density waves of perturbation in the equatorial plane where ρ_0 is the unperturbed density at each point. Parameter l/a has been chosen to be 0.25. The number in the figure denotes the time sequence of the waves. It is found that gravitational instability occurs in the cases $\gamma \gtrsim 7$ when the waves propagate inwards, and that the phase velocity of the waves is approximately equal to the sound speed.

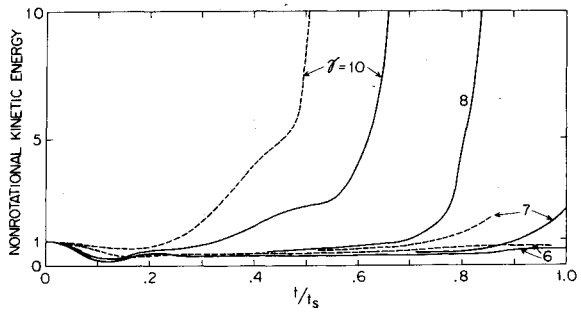

Fig. 9. The time variation of the kinetic energy of the meridional motion of the perturbed cloud in units of its initial value where $t_s(=a/c)$ is the time in which the sound wave propagates through distance a. The solid and the dashed curve represent the cases $l/a=0.25$ and 0.5, respectively. The rapid increase of the energy in the later stages is caused mainly by the excited motions in the precursor of the wave front as seen in the case $\gamma=10$ in Fig. 8.

$$\frac{dr}{dt}(t=0)=\varepsilon\frac{r}{a}\left(\frac{r}{a}-1\right)\exp\{-8(r-a)^2/l^2\}. \qquad (4\cdot29)$$

We have examined the cases $\gamma=10$, 8, 7, 6 and 4 and $l/a=0.25$ and 0.5. The calculation of motion has been carried out by use of the perturbed values of forces subtracted by the unperturbed ones in the same way as in the first test. The calculated results are shown in Figs. 8 and 9. The kinetic energy added into the equilibrium state by the form of Eq. (4·29) induces density waves up to the amount of a few percent of the unperturbed density. However, since λ/ϖ does not satisfy Eq. (4·28) initially, the density waves cannot be enhanced further but

simply propagate both in the inward and in the outward direction. In the cases $\gamma \lesssim 6$, no noticeable feature has appeared after that. In the cases $\gamma \gtrsim 7$, the density waves which propagated inwards have come to grow after ϖ decreased below some values. The kinetic energy of the meridional motion also has begun to increase exhausting the gravitational energy as shown in Fig. 9. Therefore, we may conclude that when γ is larger than some critical value, a perturbation of any wavelength can induce ring-mode instability if it does not dissipate but propagates well into the central region.

The critical value of γ probably exists between 6 and 7 and we fix it as 7 tentatively. The cause of ring-mode instability belongs to the flatness of the disk-like configuration, for the loss of the gravitational energy due to ring formation exceeds the gains of the rotation and the thermal energies. Goldreich and Lynden-Bell[11] have found that the criterion of fragmentation of isothermal, uniform surface density disk is $\lambda/z=6.7$ where λ is the wavelength and z is the thickness of the disk, which is consistent with our results because the thicknesses of our solutions are represented approximately by $z \sim \varpi/\gamma$.

§ 5. Conclusion

We have found a one-parameter family of exact solutions which describe the equilibrium of an axisymmetric isothermal cloud rotating with a constant linear velocity and also with a constant value of j/m where j is the specific angular momentum on a cylindrical surface and m is the mass contained inside the cylinder. The parameter γ represents the flatness of equi-density contours as well as the Mach number of the rotational velocity. Spacial distributions of all the quantities are conformal and, if we denote the distance from the center by l, the density is proportional to l^{-2}, the above mass m is to l and the gravity is to l^{-1}.

It has been found that nearly spherical configurations with $\gamma<2.4$ are unstable for contraction and expansion as a whole while very flattened configurations with $\gamma \gtrsim 7$ are unstable to ring formation and, probably, also to fragmentation into a few pieces. It is likely that intermediate configurations with γ lying between 2.4 and about 7 are stable.

Most of numerical computations of the collapse of rotating isothermal clouds, which have so far been performed by many people, start with the initial condition such that the ratio j/m is nearly constant. The results of many of these computations may be interpreted as that the collapse of a cloud proceeds in a direction that approaches one of the equilibrium configurations, which has the same value of j/m and that, if the value of γ of this configuration is greater than about 7, the cloud fragments into pieces in a period of one rotation or two. On the other hand, if the value of γ lies between 2.4 and about 7, the cloud can stay

in a state of near equilibrium for a longer period of time and this is interesting in connection with a study of the structure of molecular clouds. Thus, it is very important to verify the above interpretation with further numerical computations.

The above considerations are restricted to the case of isothermal clouds. Now, we consider a realistic process of star formation. After a collapsing cloud with a stellar mass becomes optically thick, the temperature rises and the gas pressure acts in a direction to decrease the flattening of equi-density contours. Then, it is expected that, if the cloud reaches an unstable equilibrium configuration with $\gamma \gtrsim 7$ before it becomes opaque, the cloud fragments to form a binary system. On the other hand, if the cloud becomes opaque before it reaches an equilibrium configuration with $\gamma \gtrsim 7$, a single star such as the sun with a surrounding pre-planetary nebula of small mass will be formed.

In the above, we have ignored completely the effect of magnetic fields. The study of transport of angular momentum as discussed, for example, by Hayashi[2] will be important before we obtain a final answer to the problems of star formation and planetary formation. For this purpose, however, the physics of collapse without magnetic effects is to be clarified at first.

Acknowledgements

The numerical calculations were performed by FACOM M-200 at the Data Processing Center of Kyoto University. This work was supported by the Grant-in-Aid for Scientific Research of the Ministry of Education, Science and Culture (No. 56110009).

References

1) P. Bodenheimer, *Fundamental Problems in the Theory of Stellar Evolution* (Proc. IAU Symposium No. 93, 1981), ed. by D. Sugimoto et al., (Reidel Pub., Holland), p. 5.
2) C. Hayashi, Prog. Theor. Phys. Suppl. No. 70 (1981), 35.
3) S. Narita, D. McNally, G. L. Pearce and S. A. Sørensen, Month. Notices Roy. Astron. Soc. to be published.
4) D. Wood, Month. Notices Roy. Astron. Soc. **194** (1981), 201.
5) M. L. Norman, J. R. Wilson and R. T. Barton, Astrophys. J. **239** (1980), 968.
6) L. Mestel, Month. Notices Roy. Astron. Soc. **126** (1963), 553.
7) R. B. Larson, Month. Notices Roy. Astron. Soc. **145** (1969), 271.
8) L. Spitzer, *Physical Processes in the Interstellar Medium* (Wiley-Interscience, New York, 1978).
9) A. P. Boss and J. G. Haber, Astrophys. J. **255** (1982), 240.
10) D. Wood, Month. Notices Roy. Astron. Soc. **199** (1982), 331.
11) P. Goldreich and D. Lynden-Bell, Month. Notices Roy. Astron. Soc. **130** (1965), 7, 125.

Note added in proof: After we submitted this paper, a paper by Toomre (Astrophys. J. **259** (1982), 535) appeared. He also found the same solutions as Eq. (2·3), although he did not study the stability of the equilibrium configurations.